Structure, Vol. 10, 51–60, January, 2002, ©2002 Elsevier Science Ltd. All rights reserved. PII S0969-2126(01)00699-2

Probing Substates in Sperm Whale Myoglobin Using High-Pressure Crystallography

Paul Urayama,[1,4] George N. Phillips, Jr.,[2] and Sol M. Gruner[1,3]
[1]Department of Physics
Cornell University
Ithaca, New York 14853
[2]Department of Biochemistry
University of Wisconsin
Madison, Wisconsin 53706

Summary

Pressures in the 100 MPa range are known to have an enormous number of effects on the action of proteins, but straightforward means for determining the structural basis of these effects have been lacking. Here, crystallography has been used to probe effects of pressure on sperm whale myoglobin structure. A comparison of pressure effects with those seen at low pH suggests that structural changes under pressure are interpretable as a shift in the populations of conformational substates. Furthermore, a novel high-pressure protein crystal-cooling method has been used to show low-temperature metastability, providing an alternative to room temperature, beryllium pressure cell-based techniques. The change in protein structure due to pressure is not purely compressive and involves conformational changes important to protein activity. Correlation with low-pH structures suggests observed structural changes are associated with global conformational substates. Methods developed here open up a direct avenue for exploration of the effects of pressure on proteins.

Introduction

Pressures encountered in the biosphere, up to 120 MPa in the deepest oceans, have large effects on biological systems. Proteins show changed kinetic and equilibrium constants, multimeric associations, folding profiles, and ligand bindings; membranes show altered permeability. Cellular metabolism, cellular morphology, and viral infectivity may also be affected [1–5]. Such phenomena at moderate pressures might appear paradoxical because proteins have small intrinsic compressibilities (10^{-5} to 10^{-6} MPa^{-1} for globular proteins) [6–9] and tightly packed interiors [10]. Thus, detailed structural and dynamical information are also needed in understanding pressure effects in proteins.

Probes adapted for high pressure include spectroscopy and fluorescence, NMR, circular dichroism, and small angle X-ray scattering [5]. However, the one least developed for high pressure is the one most powerful at giving atomic level information—X-ray crystallography. One reason for the lack of development is the perception that protein crystals do not survive pressurization well. Studies on lysozyme [11–13], staphylococcal nuclease [14], and myoglobin [15, 16] show that protein crystals are more robust than typically thought. Here, we show that pressure may even make the crystal more robust in certain circumstances, such as during cooling.

Another reason for the slow development of high-pressure crystallography is the difficulty in obtaining high-pressure data. Kundrot and Richards [11] used a dead end-bored beryllium rod mounted on a goniometer as an X-ray transparent pressure vessel for crystals in the 100 MPa range. Later, Tilton [17] modified the design for 10 MPa range gas pressures. The main disadvantage, however, was that beryllium has strong powder diffraction rings at crystallographically important resolutions starting at about 2 Å. To surmount such difficulties, we developed a cooling method in which the protein crystal was cooled while under pressure, with the goal of "freezing-in" pressure-induced collective movements of the polypeptide chain. The crystal was not under pressure during diffraction, though the crystal was at cryogenic temperatures. Unlike in flash cooling, no chemical cryoprotectant (for example, glucose or sucrose) was used, even though the cooling rate was slow ($\sim$2 K/s).

When observing the effects of pressure, it is important to remember that a crystallographic structure is an ensemble structure. This has implications when we divide observed changes into *conformational* and *elastic* components. Here, elastic effects are ones in which the changes in the conformation of groups of atoms may be described by a simple isotropic expansion or compression of the molecule. Proteins have many low-energy conformations, and pressure acts to change the population of those conformations. Crystallographic observations most likely reflect the ensemble average of the change in substate populations.

The existence of hierarchical conformational and energy landscapes in proteins is well established [18, 19]. Substates in carbonmonoxy-myoglobin (CO-myoglobin or MbCO) are represented by those monitored by IR stretch bands of bound CO at $\nu(A_0) \approx 1967\ cm^{-1}$, $\nu(A_1) \approx 1947\ cm^{-1}$, and $\nu(A_3) \approx 1929\ cm^{-1}$ [20]. These *taxonomic substates* may have different reactive properties [21], making the ability to characterize the structure of substates important in understanding reaction mechanisms.

The equilibrium ratio w_0/w_1 of substate populations depends on the free energy difference $\Delta G = G_0 - G_1$ between substates, namely as

$$\frac{w_0}{w_1} = e^{-\frac{\Delta G}{RT}} = e^{-\frac{\Delta E + P\Delta V - T\Delta S}{RT}} \quad (1)$$

where ΔE, ΔV, and ΔS are the differences in the internal energy, volume, and entropy of the conformations. Thus, pressure shifts the population by a factor $\exp[-P\Delta V/RT]$ [22].

[3]Correspondence: smg26@cornell.edu
[4]Present address: Department of Physics and Astronomy, Dartmouth College, Hanover, New Hampshire 03755.

Key words: myoglobin; pressure; pH; conformational substates; metastability; cryocrystallography

Table 1. Data and Refinement Statistics

	RTRP(MYO2)	RTHP(MYOCE)	LTHP(MYO3)	LTHP(MYO4)	
A. Data collection					
Temperature, K	295	295	95	95	
Pressure, MPa	0.1	150	200	200	
pH	6	6	6	6	
Cell dimensions					
a ± 0.11 Å	64.45	64.09	64.08	63.87	
b ± 0.04 Å	30.93	30.80	30.78	30.76	
c ± 0.04 Å	34.73	34.57	34.40	34.43	
β ± 0.1°	105.7	105.7	105.4	105.5	
vol ± 170 Å^3	66640	65680	65410	65160	
Mosaicity, °	–	–	0.27	0.31	
Resolution range, Å	9.2–2.3	9.2–2.3	26.0–1.7	26.5–1.7	
(highest shell)*	(2.48–2.30)	(2.42–2.30)	(1.81–1.67)	(1.79–1.68)	
Completeness*, %	96.9 (94.5)	90.1 (79.6)	98.5 (97.7)	98.7 (99.0)	
Multiplicity*	2.6 (2.0)	2.9 (2.4)	4.0 (3.6)	2.9 (2.8)	
Mean* I/σ	14.7 (15.6)	12.1 (6.0)	4.8 (6.8)	3.8 (8.8)	
R_{means}*, %	4.4 (5.6)	5.7 (13.8)	7.5 (9.6)	7.2 (8.4)	
B. Refinement					
Refinement range, Å	9.2–2.3	9.2–2.3	26.0–1.7	26.5–1.7	
Reflections, I/σ > 2	5853	5306	14240	14137	
R, %	16.0	16.6	21.0	21.0	
R_{free}, %	21.7	23.5	24.7	23.8	
Rmsd bond lengths, Å	0.006	0.006	0.005	0.005	
Rmsd bond angles, °	1.021	1.004	0.975	0.969	
Real space fit	0.062	0.060	0.068	0.084	
*Highest resolution shell in parentheses					

	1VXH*	RTRP(r1VXH)	1VXE*	1VXB*	1A6K†
A. Data collection					
Temperature, K	277		277	277	90
Pressure, MPa	0.1		0.1	0.1	0.1
pH	6		5	4	7
Cell dimensions					
a, Å	64.46		64.52	64.35	63.90
a, Å	30.89		30.85	30.92	30.73
a, Å	34.76		34.77	35.53	34.36
β, °	105.91		106.1	106.8	105.7
vol, Å^3	66560		66490	67710	64950
B. Refinement					
Refinement range, Å	5.0–1.7	31.0–1.8	5.0–1.7	5.0–2.0	8.0–1.1
Reflections, no cutoff	13856	12293 (I/σ > 2)	13807	7156	51286
R, %	14.0	17.7	15.6	20.0	13.2
R_{free}, %	N/A	19.8	N/A	N/A	15.2
Rmsd bond lengths, Å	0.026	0.005	0.024	0.025	0.018
Rmsd bond angles, °	1.964	0.988	1.865	2.298	2.482
Real space fit	N/A	0.053	N/A	N/A	N/A
*From [24]					
†From [28]					

Ansari et al. [20] and Frauenfelder et al. [22] have characterized population ratios in solution for a range of pH, temperature, and pressures. Lower pH and higher pressure increase the A_0 population with respect to A_1. At room temperature and pressure, a pH change from 6.6 to 5.5 increases the ratio A_0/A_1 by about an order of magnitude. At room temperature, a pressure increase from 0.1 MPa to 200 MPa increases the ratio A_0/A_1 by a factor of 2.8 at pH 6.6, and a factor of 1.9 at pH 5.5.

The correlation between structure and spectroscopic A tier substates in MbCO is well studied for various pH [20, 23–26]. The low-pH A_0 form is associated with an "open" conformation, in which His64 is protonated and rotated out of the heme pocket. The substates may also have slightly varying CO tilt angles.

Less attention has been paid to global aspects of substate conformations in myoglobin, although molecular dynamics simulations of myoglobin have revealed global conformational substates [19]. Can the global differences between conformational substates be determined experimentally? This is especially important because myoglobin can be described as an "allosteric" enzyme with ligand binding and unbinding affected by conformational substates [21].

The purpose of this paper is two-fold. First, we describe techniques for high-pressure crystallography by characterizing pressure-induced changes in sperm whale myoglobin up to 200 MPa and evaluating whether low temperatures successfully lock in relevant pressure-induced structural changes when cooled under pressure.

Second, we describe conformational substates in myoglobin by comparing observed structural changes

Table 2. Evolution of Rmsd's during Refinement

2.3 Å resolution set RTRP(MYO2)			
Resolution (Å)	R (R_{free}) (%)	Rmsd (Å) compared with reference structure	
2.3	22.8 (30.0)	0.111	
2.3	19.1 (25.8)	0.080	
2.3	16.6 (22.7)	0.047	
2.3	16.0 (21.7)	reference	
2.3	15.9 (21.7)	0.050*	
2.3	17.1 (24.3)	0.085†	
1.7 Å resolution set LTHP(MYO3)			
Resolution (Å)	R (R_{free}) (%)	Rmsd (Å) compared with reference structure	
2.0	26.2 (31.1)	0.212	
1.8	23.3 (27.0)	0.077	
1.7	21.6 (25.4)	0.042	
1.7	21.1 (25.0)	0.026	
1.7	21.0 (24.7)	reference	
High-resolution sets in similar stages of refinement LTHP(MYO3, MYO4)			
Resolution (Å)	R (R_{free}) MYO3 (%)	R (R_{free}) MYO4 (%)	Rmsd (Å)
2.0	26.3 (31.3)	26.2 (31.1)	0.188
1.8	22.9 (26.7)	23.3 (27.0)	0.155
1.7	21.6 (25.4)	21.6 (24.4)	0.106
1.7	21.0 (24.7)	20.9 (23.8)	0.098

*After two extra cycles of 3000 K simulated annealing
†After two extra cycles of 5000 K simulated annealing

at various pH values [24] with those at various pressures. Carbon monoxide spectroscopic shifts in A_0/A_1 ratios are compared with pH- and pressure-induced structural changes.

Results and Discussion

Table 1 summarizes structures discussed in this paper. Structure nomenclature includes the temperature (RT, room temperature; LT, low temperature), the pressure (RP, room pressure; HP, high pressure), and the data set reference in parentheses (e.g., "MYO2"). The prefix "MYO" indicates structures solved here. A four-letter identifier indicates structures taken from the Protein Data Bank (PDB) [27]. These are 1A6K from Vojtechovský et al. [28] and 1VXH, 1VXE, and 1VXB from Yang and Phillips [24]. All structures were in the aquometmyoglobin (met-Mb) form.

We evaluated low-temperature metastability through high-pressure cooling by comparing differences between structures RTRP(MYO2) and RTHP(MYOCE) with differences between structures LTRP(1A6K) and LTHP(MYO3).

Next, we compared global structural changes at low pH and high pressure, both of which have increased A_0/A_1 ratios when observed spectroscopically. The pH comparison was between the pH 4 structure RTRP(1VXB) and the pH 6 structure RTRP(1VXH). The pressure comparison was between the 0.1 MPa structure RTRP(MYO2) and the 150 MPa structure RTHP (MYOCE).

Analysis focused on determining collective displacements in the peptide backbone and rearrangements of secondary structural elements.

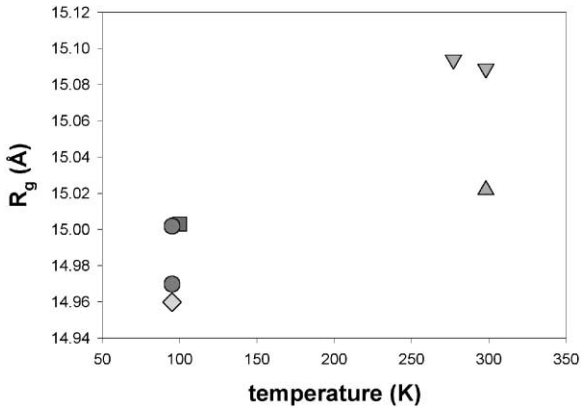

Figure 1. Radius of Gyration before Isotropic Scaling Calculated Using Extended Main Chain Atoms of the First 151 Residues

The pressures were as follows: 0.1 MPa (upside down triangle, square), 150 MPa (right side up triangle, diamond), and 200 MPa (circle).

Detectability and Robustness of Backbone Positions

To determine the detectability of changes and the reproducibility of backbone positions for sperm whale myoglobin, we looked at differences between refined structures from crystals under similar conditions and at changes in atomic positions during structural refinement.

Structures 1VXH and 1VXE were met-Mb structures at pH 6 and pH 5, respectively, and had no significant changes as compared with a pH 4 structure 1VXB [24]. We found that 1VXH and 1VXE had a root-mean-square difference (rmsd) in extended main chain (i.e., N, C, O, and C_α) atom positions of 0.102 Å. For another ambient condition comparison, the rmsd between RTRP(MYO2) and RTRP(r1VXH) was 0.113 Å. For high-pressure cooled sets LTHP(MYO3) and LTHP(MYO4), the rmsd was 0.094 Å. LTRP structures under similar conditions were not available for comparison.

Next, we looked at sources for error during model refinement. Differences in starting coordinates and tar-

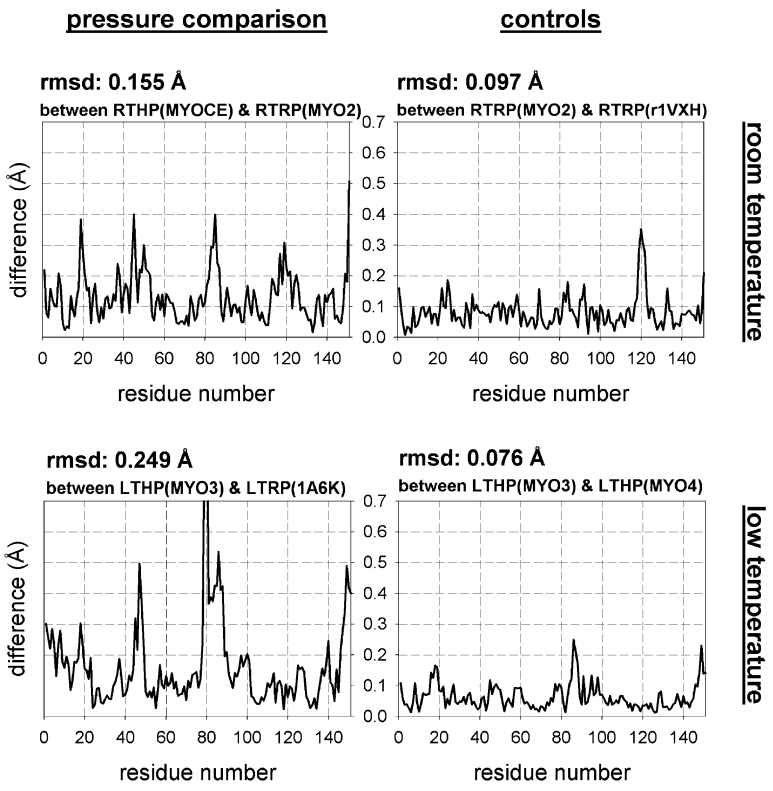

Figure 2. Change in Position of the Center of Mass of Residue *i* Calculated from Extended Main Chain Atoms of the First 151 Residues after Isotropic Scaling

Changes are differences in residue positions after least squares superpositioning. The top figures show pressure comparison and control at room temperature. Structures superposed were RTHP(MYOCE) and RTRP(MYO2), and RTRP(MYO2) and RTRP(r1VXH), respectively. The bottom figures show the pressure comparison and control for low-temperature structures. Comparisons were between LTHP(MYO3) and LTRP(1A6K), and LTHP(MYO3) and LTHP(MYO4), respectively.

get functions may give differences which, while not important in solving gross protein structure, may be important when comparing small differences. Two structures refined from the same structure factors, RTRP(1VXH) refined using X-PLOR v3.1 ($R = 14.0\%$, R_{free} not given) and RTRP(r1VXH) refined in-house using CNS v1.0 ($R = 17.7\%$, $R_{free} = 19.8\%$), had an rms difference of 0.095 Å in extended main chain atom positions.

We estimated the effect of incorrect side chain geometry by taking the LTHP(MYO3) model and mutating side chains to either alanine or glycine, depending on whether there was a C_β in the original residue. The R factors after two cycles of 3000 K simulated annealing with torsional dynamics, followed by conjugate gradient minimization, where $R = 34.0\%$ and $R_{free} = 38.0\%$ for the truncated LTHP(MYO3) model. Compared with the original LTHP(MYO3) structure, the rmsd in extended main chain atom positions was 0.127 Å. Thus, backbone atom positions appear quite robust in the presence of side chain errors.

Changes in the model during different stages of refinement must also be considered, as R factors and diffraction resolution may have an effect on backbone positions. Table 2 shows rmsd's in extended main chain atoms during refinement. Below R_{free}'s of 30%, rmsd's quickly fall to below rmsd's seen between well-refined structures. Below R_{free}'s of 25.0%, rmsd's between refinement cycles are about 0.05 Å.

Even a poorer resolution structure RTRP(MYO2), in which refinement was to 2.3 Å, had robust backbone coordinates. After two additional 3000 K simulated annealing cycles with Cartesian refinement (instead of torsional refinement), the rmsd in the extended main chain backbone was 0.050 Å when compared with the original structure. When additional annealing cycles were at 5000 K, the rmsd was 0.085 Å.

This suggests that positions of main chain atoms were well established early in refinement, provided that stereochemical errors were corrected during structure validation. We considered structures with R_{free}'s of 25% or less to have backbone positions determined to the level in which refinement errors and natural variability could not be distinguished, at least for the case of $P2_1$ sperm whale myoglobin crystals.

Considering rmsd's between similar structures and the evolution of differences during refinement, we estimated that displacements of greater than 0.1 Å in the backbone were significant. Such an estimate does not apply to side chain atoms, which may show more uncertainty.

Isotropic versus Anisotropic Changes

In characterizing collective changes in structure, it was useful to separate isotropic (elastic or compressive) and anisotropic (conformational) effects. The small intrinsic compressibility of proteins [3, 9] suggests that isotropic effects may be small and would have to be carefully distinguished from anisotropic changes such as rearrangements of internal structural elements.

Data for LTHP structures were taken at ambient pressures, so anisotropic changes could be frozen-in while compressive changes had relaxed. Thus, the effect of pressure on internal cavity volumes could not determined. Figure 1 shows the radius of gyration, R_g, for various structures, calculated using the extended main chain atoms of the first 151 residues. The last two residues, Gln152 and Gly153, were often disordered and

do not consistently appear in crystallographic electron densities. The RTHP structure showed compressive change, but the wide range of R_g's for LTHP structures suggested possible compressive relaxation upon pressure release.

A simple gas-like model was used to characterize isotropic differences by assuming a scaling in which distances between atoms remained proportional, that is,

$$\mathbf{r}_i - \mathbf{r}_j = \left[\frac{V}{V'}\right]^{\frac{1}{3}} (\mathbf{r}_i' - \mathbf{r}_j') = \frac{R_g}{R_g'}(\mathbf{r}_i' - \mathbf{r}_j'), \qquad (2)$$

where V and R_g are the crystallographically determined molecular volume and radius of gyration and primes refer to the data set to be scaled. Note, by scaling molecular volumes, we assumed the topology of the protein did not change. This is a valid approximation for small changes, as was the case here; indeed, Figure 1 shows that R_g's differed by less than 1%. Such a scaling is sensitive to purely isotropic effects. Equation 2 does not preserve bond lengths, but does preserve relative orientation of atoms. Structures in subsequent analyses were scaled to V and R_g of RTRP(MYO2).

Identifying Collective Movements

We superposed scaled structures using only extended main chain atoms of the first 151 residues. Superpositions and rmsd values were calculated using LSQMan [29]. Figure 2 shows displacements as a function of residue. The residue's position was taken to be the center of mass (COM) of extended main chain atoms in that residue. The rmsd's between pressure comparisons were greater than for controls.

Because we were interested in rearrangements of *groups* of residues (for example, of α helices), we applied a smoothing algorithm to highlight robust features in Figure 2. Figure 3 shows displacements seen by letting the position of residue i be the COM of the $(i - n)$ to $(i + n)$ residue. COM calculations included only extended main chain atoms and the window shifted along the first 151 residues excluding the end residues with no neighbors. Six regions showed large collective displacements. These were the A helix, AB loop, CD loop, F helix, GH loop, and H helix. Most other regions had differences at the level of detectability, deemed to be about 0.1 Å; thus, further discussions will focus on these six regions.

Low-Temperature Metastability: Pressure Comparisons at Room and Low Temperatures

To display the spatial movements of the six regions (A helix, AB loop, CD loop, F helix, GH loop, and H helix), we used the same smoothing procedure as was used to calculate COM displacements as a function of residue between two structures. The atmospheric structure was then morphed by applying the COM displacement, multiplied by an amplification factor, to the entire residue. This was implemented in Mathematica code, and the results are in Figure 4.

Under pressure at room temperature, the F helix slid along its axis and moved toward the E helix. The AB loop moved toward the E helix. The CD loop slid toward the D helix and the G and H helix regions. Of smaller magnitude were displacements of the H helix toward

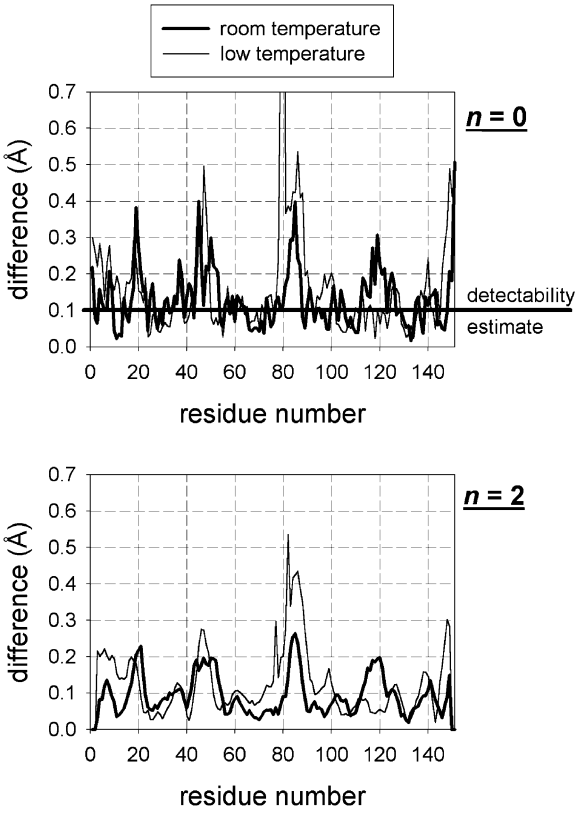

Figure 3. Robust Displacements Are Identified by Smoothing (See Text for Procedure)

Zero and two neighbors (one and five residues total, respectively) were used to calculate the COM. Coordinates have been isotropically scaled to RTRP(MYO2). The 0.1 Å detectability estimate is drawn in for comparison. The thick line is between RTRP(MYO2) and RTHP(MYOCE), and the thin line is between LTRP(1A6K) and LTHP(MYO3).

the G helix, the GH loop toward the A helix, and the A helix away from the E helix.

Comparing flash-cooled room pressure and high-pressure cooled structures, the F helix slid along its axis and moved toward the E helix. The AB loop moved toward the E helix. The CD loop moved towards the D helix and fanned out. Of smaller magnitude were displacements of the H helix toward the G helix except at the carboxy-terminal end, and of the A helix toward the E helix.

Thus, the AB loop, F helix, and H helix showed similar pressure-induced displacements for room temperature and low-temperature sets. The CD loop appeared to move toward the D helix at both temperatures. However, at room temperature, the CD loop also moved toward the G and H helices, while at low temperature, the loop fanned out.

The A helix and GH loop pressure responses were not similar between room and low temperatures. The GH loop appears to be a naturally variable region, however. For example, the room temperature control plot in Figure 2 had a peak in that region.

We looked at the cosine of the angle between displacement vectors from the two temperatures as a function of residue to evaluate how similar the pressure dis-

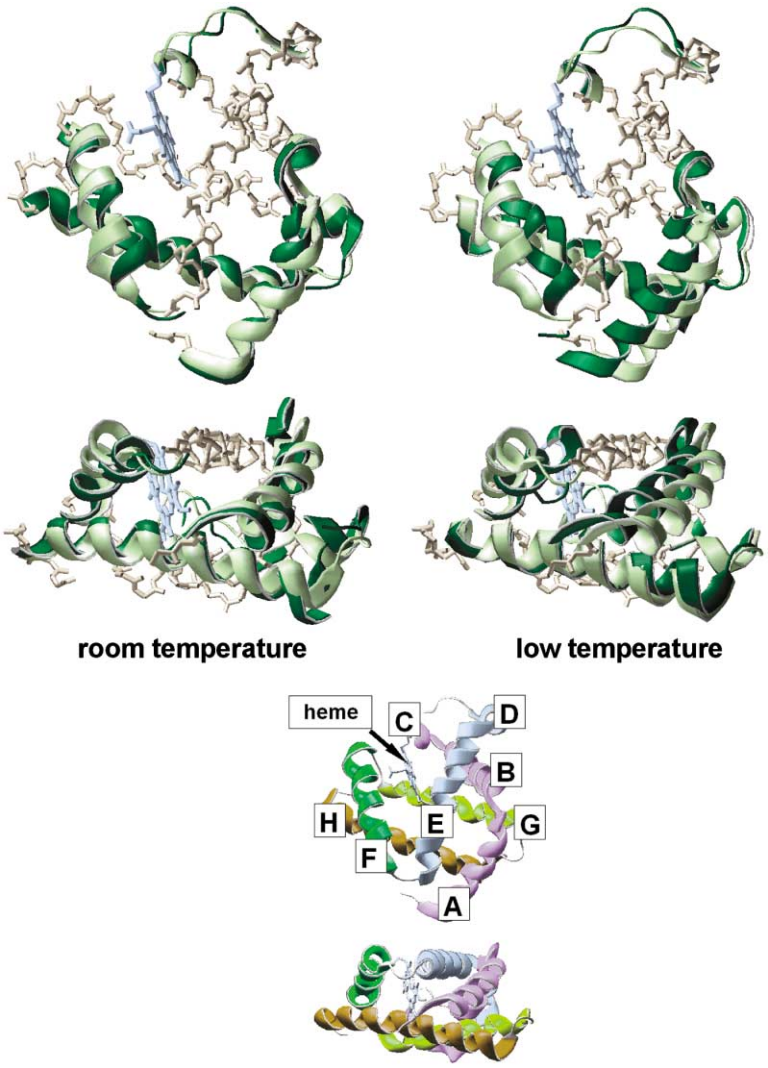

Figure 4. Comparison of Pressure-Induced Displacements at Room Temperature (Top, Left) and Low Temperature (Top, Right)

Regions rendered as ribbons are residues 3–24, 40–52, 79–94, and 115–147. Only extended main chain atoms are shown for all other residues. Structures are orthogonally oriented along principal axes, with the structures (middle) rotated 90° along the horizontal axis. Displacements have been amplified by a factor of 15. Light shading indicates ambient pressure positions. Dark shading indicates high-pressure positions. The figures at the bottom are a key to the labeling of the helices.

placements were at ambient and low temperatures. A positive value indicated the displacement vectors at the two temperatures were correlated (angle less than 90°), and a negative value indicated the displacement vectors at the two temperatures were anticorrelated (angle greater than 90°). Though there were significant regions where the cosines anticorrelate, it was important to consider whether differences in position were significant, that is, greater than the 0.1 Å detectability estimate. For this, we considered the dot product of the pressure-induced displacement vectors for the two temperatures, that is,

$$\vec{r}_{i,lowT} \cdot \vec{r}_{i,roomT} = r_{i,lowT} r_{i,roomT} \cos\theta_i, \quad (3)$$

where $\vec{r}_i$ is the displacement vector between residues of room pressure and high-pressure structures and θ_i is the angle between the vectors. Thus, letting $r = 0.1$ Å, a $\vec{r}_{lowT} \cdot \vec{r}_{roomT} > 0.01$ Å^2 is necessarily significant, since $|\cos q| \leq 1$. Using this criterion, regions that showed significant correlations were the AB loop, CD loop, F helix, and the region of the H helix nearest the F helix. Regions that showed significant differences were the A helix and the region of the H helix nearest the A helix.

Similarities in the largest displacement regions were evidence for low-temperature metastability. The reason for small differences may be that crystals for structures LTRP(1A6K) and LTHP(MYO3) were not cooled at the same rate. Rates for flash cooling were between 50 and 700 K/s [30] and the rate for high-pressure cooling was 1.7 K/s. We did not explore the effects of high-pressure cooling rates because it was difficult to change the thermal mass of the pressure cell. A high-pressure flash cooling protocol is being developed.

Probing Conformational Substates: pH and Pressure Comparisons

We compared differences between RTRP(1VXB) and RTRP(1VXH) with differences between RTRP(MYO2) and RTHP(MYOCE). Structures were isotropically scaled to RTRP(MYO2). Figure 5 shows the differences in the COM positions of extended main chain atoms of the first 151 residues for pH and pressure comparisons at or near room temperature. Note the larger rmsd for the

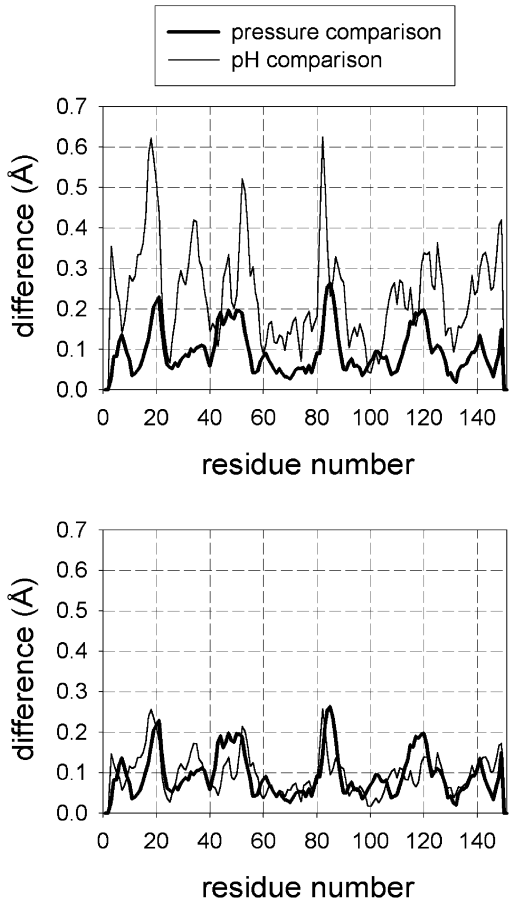

Figure 5. Displacement in Backbone Positions upon Change in pH and Pressure

Robust displacements are identified by smoothing (see text for procedure). Two neighbors (top) are used to calculate the COM. Coordinates have been isotropically scaled to RTRP(MYO2). The thick line is between RTRP(MYO2) and RTHP(MYOCE), and the thin line is between RTRP(1VXB) and RTRP(1VXH). The bottom figure shows the displacements after scaling rmsd's.

pH comparison, consistent with larger changes in A_0/A_1 ratios observed spectroscopically. After scaling rmsd's, the differences tracked well.

Figure 6 shows the spatial displacements of the six regions (A helix, AB loop, CD loop, F helix, GH loop, and H helix) using the same smoothing procedure as in Figure 4. The amplification factors were chosen to scale rmsd's and were 6.2 for the pH comparison and 15 for the pressure comparison.

Both low-pH and high-pressure structures showed a steepening of the A helix angle with the N-terminal end moving away from the E helix, displacement of the AB loop toward the E helix, opening of the CD loop toward the D helix, sliding of the F helix along its axis and toward the E helix, and displacement of the H helix toward the G helix.

We did not observe an "opening" of the His64 residue, which Yang and Phillips only observed in the MbCO low-pH structure, not the met-Mb structure. However, there were large displacements in the CD loop, suggesting an opening in the distal heme region.

Yang and Phillips report a peptide bond flip between Lys79 and Gly80 in their pH4 MbCO structure (PDB 1SPE). Interestingly, though we did not observe such a flip in the room temperature pressurized structure RTHP(MYOCE), we did observe the flip in the high-pressure cooled samples LTHP(MYO3) and LTHP(MYO4).

Previously, studies of conformational substates have focused mainly on the heme pocket, namely at the orientation and the protonation state of His64 and His97 [20, 23–26, 31, 32]. The similarity between low-pH and high-pressure structural changes and the corresponding spectroscopically observed shifts in A_0/A_1 populations suggest that high-pressure probes have global substate properties.

A global structural probe for substates is especially important in light of the realization that myoglobin has nonexponential binding properties that arise from its heterogeneous substate populations [33–38] and that these substates may have differing reaction properties [21]. Because such correlations exist even in the met form (the CO form as used in the majority of studies), the structural rearrangements presented here may have more general significance.

Biological Implications

Pressures accessible in the biosphere have large effects on organisms, as some species have adapted to particular pressures or range of pressures; for example, many deep sea fishes are obligate barophiles. These effects may eventually be traced to effects on the molecular level, such as on changes in protein structure, because pressure affects reaction rates, equilibrium constants, and folding stability. Though many structural probes have been developed for use under pressure, the technique most powerful at giving atomic level information, X-ray crystallography, is the one least utilized.

Here, we present a 150 MPa structure of sperm whale myoglobin. We also developed a method for cooling a protein crystal under pressure with the goal of "freezing-in" pressure-induced structural changes. This provides an alternative to room temperature, beryllium pressure cell-based techniques for which the pressure cell has strong powder diffraction at crystallographically important resolutions. Finally, we interpret observed structural changes in terms of conformational substates by comparing pressure-induced structural changes with those observed at low pH.

Comparing the effects of pressure at room and low temperatures shows that the largest of the structural reorientations in sperm whale myoglobin are preserved when cooled under pressure. These are displacements in the F helix, AB loop, and CD loop regions. The main dissimilarity is in the A helix region. Note that the high-pressure cooled crystals were *not* under pressure during X-ray data acquisition. That the differences between ambient and high-pressure structures at low and ambient temperatures are similar implies that high-pressure cooling locks in features seen in *actively* pressurized proteins, making possible high-resolution pressure studies of protein conformations.

The population of spectroscopically identified conformational substates in myoglobin is known to change

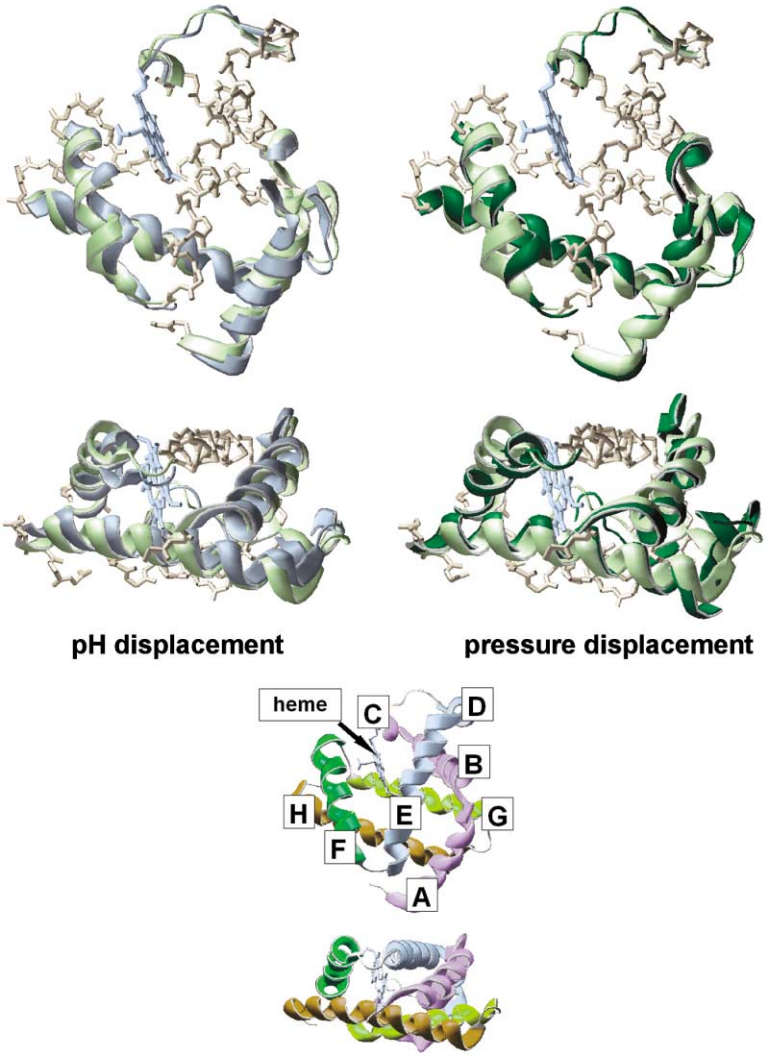

Figure 6. Comparison of Displacements at Low pH (Top, Left) and High Pressure (Top, Right)

Regions rendered as ribbons are residues 3–24, 40–52, 79–94, and 115–147. Only extended main chain atoms are shown for all other residues. Structures are orthogonally oriented along principal axes, with the structure (middle) rotated 90° along the horizontal axis. Displacements have been amplified by a factor of 6.2 (left) and 15 (right). Light shading indicates ambient pressure positions. Dark shading indicates low-pH or high-pressure positions. The figures at the bottom are a key to the labeling of the helices.

in a similar manner when lowering pH and increasing pressure [22]. A comparison of low-pH and high-pressure structures also shows good correlation. This implies that, despite their many degrees of freedom, the global protein conformation has energy minima distinct enough to be identified as conformational substates, consistent with results from molecular dynamics simulations [19]. Rejto and Freer [39] reviewed crystallographic methods for studying protein substates. Here, we demonstrate the feasibility of high-pressure crystallography for providing additional substate data.

Myoglobin is expected to be a particularly challenging protein for pressure studies because it is small and compact and, consistent with the Kundrot and Richards [6] pressure study of lysozyme, exhibits only small structural responses to pressure. Even so, as shown in this article, the small structural changes under pressure can be interpreted in terms of other structural data such as spectroscopy in understanding conformational substates. There is every reason to believe that the techniques used here to study myoglobin may also be used to help reveal the mechanisms of pressure-induced functional changes in other proteins.

Recent near-atomic resolution structures of sperm whale myoglobin in various ligated forms [28, 40] and high-pressure Raman studies [41] also suggest the importance of rigid body movements in the F helix region. Thus, the determination of variously ligated, high-pressure myoglobin structures would lead to a fuller description of substates that could be connected to spectroscopic and kinetic data.

Experimental Procedures

Crystallization Protocol

$P2_1$ crystals of sperm whale myoglobin (Sigma; acquired before the ban on commercial trade of sperm whale products) for structures solved here were grown at room temperature in batch mode from 72%–78% saturated ammonium sulfate (A.S.), unbuffered. The solution was between pH 5.5 and 6.0, and the myoglobin was in the met form.

Room Temperature Beryllium Cell Technique

Structure RTHP(MYOCE) came from a crystal mounted inside a Kundrot-Richards-type beryllium cell [11]. The cell is essentially the same as the Kundrot and Richards design, except that we modified the high-pressure seal to go to higher pressure and used beryllium grade I-250 (2.5% BeO content) rather than I-400 (4.2% BeO content; Brush-Wellman). The lower BeO content improved X-ray transmittance without the loss of metal strength. The cell mounts directly onto a goniometer.

The pressure used was 150 MPa ± 1% as read by a piezoresistive transducer (Sensotec). The cell connected to a manually operated piston pressure generator (High Pressure Equipment Company) via flexible syringe tubing.

High-Pressure Cooling Technique

Structures LTHP(MYO3) and LTHP(MYO4) came from crystals prepared using a high-pressure cooling technique modified from Thomanek et al. [15]. They cooled myoglobin crystals at 250 MPa as a method for protecting the crystal against damage caused by ice formation during slow cooling, which would normally destroy the crystal. After cooling in liquid nitrogen, the pressure was removed while the crystal was kept cold. They reasoned that such pressures would freeze water to ice III, which contracts, in contrast with ice Ih, which expands. Although diffraction data was collected, to the best of our knowledge there was no further development of their technique and no structures were published. Here, we used pressures between 150 and 200 MPa, which is below the ice III region, thereby ruling out the Thomanek hypothesis for the protection effect. Our method allowed the frozen crystal to be mounted in a standard cold stream for routine protein crystallographic data collection.

The pressure vessel used during cooling was a commercially available stainless steel 1/8″-to-1/4″ high-pressure couple (High Pressure Equipment Company) with two cone-sealed ends and a central bore. The couple connected to a manually operated piston pressure generator (High Pressure Equipment Company).

During pressurization and cooling, the crystal was held in the central bore of the couple. Because it was not possible to remove the crystal from solid ice, the pressurizing medium was isopentane instead of mother liquor. After pressurization, the pressure vessel was immersed in liquid nitrogen until all bubbling ceased outside the vessel. The pressure was then released and the pressure vessel was disassembled at liquid nitrogen temperatures. When cooled at rates used here (1.7 K/s), isopentane was a glassy, gelatinous solid, making removal from the cooled pressure vessel possible using a pushpin jig. When left for several hours at liquid nitrogen temperatures, isopentane crystallized into a powder that flaked from the crystal. Isopentane is immiscible in water, so it did not dehydrate the crystal. Crystals were in saturated A.S. before being placed in isopentane, and the solution contained no chemical cryoprotectants.

Once cooled under pressure and removed from the pressure cell, the crystal was put into an X-ray capillary and held in place between bits of sponge (found as packing material for microscope glass coverslips). The capillary was bonded to the steel post of a magnetic CrystalCap base (Hampton Research) using cyanoacrylate adhesive. Once mounted in this way, the crystal was compatible with existing cryogenic storage and handling protocols [42]. Because the crystal could not be warmed after being cooled under pressure, the crystal was kept in contact with liquid nitrogen or a cooled copper stage mostly immersed in liquid nitrogen. Note, incidentally, that myoglobin crystals without cryoprotectants do not freeze well by most conventional flash-freezing protocols even where cooling rates were higher (50–700 K/s measured by Teng and Moffat) [30].

Crystals were at high pressure for at least 90 min before cooling. Cooling rates were 1.7 K/s as measured by a thermocouple placed at the sample. The pressure used was 200 MPa ± 1% as read by a piezoresistive transducer (Sensotec). Mosaicities of high-pressure cooled crystals were comparable to or only slightly higher than mosaicities of crystals prepared by cryoprotected flash cooling.

Data Collection and Reduction

Data for room temperature structures were collected on a rotating anode source using an ADSC multiwire area detector. Data for cooled crystals were collected at Cornell University's CHESS F1 line using an ADSC Quantum 4 CCD-based detector. Data reduction was preformed using the DPS [43] and/or CCP4 [44] packages.

Ambient Pressure and Low-pH Data Sets

We used the glass capillary-mounted RTRP(MYO2) as the room temperature control and deposited the 1VXH and 1VXE structures (pH 6 and 5, respectively) as additional RTRP checks in the Protein Data Bank.

The low-temperature, ambient pressure structure was the PDB-deposited aquometmyoglobin structure 1A6K. The preparation technique is described in Vojtechovský et al [28].

The pH 4 structure was the Protein Data Bank-deposited aquometmyoglobin structure 1VXB. The preparation technique is described in Yang and Phillips [24].

Refinement

Table 1 summarizes refinement statistics for the four structures determined here. Data set 1VXH coordinates were used as starting coordinates for refinement. Refinement using CNS version 1.0 [45] involved rigid body refinement at low resolution (3.0 Å), followed by 3000 K simulated annealing at 2.2 or 2.3 Å. Higher resolution data, if present, were added in cycles of minimization and restrained, individual B factor refinement. A randomly chosen test set (10% of reflections) served in calculating the crossvalidated R factor [46].

Heme, sulfates, and waters were added during manual model building using O version 6.2.1 [47]. In adding waters, $2F_o–F_c$ and $F_o–F_c$ maps were inspected at 1σ and 3σ, respectively, and positions were checked for hydrogen-bonding geometry.

Structure validation using PROCHECK [48] revealed a Ramachandran plot outlier, Lys79, in the LTHP structures. Inspection of $2F_o–F_c$ maps showed the peptide bond between Lys79 and Gly80 had flipped. In the structure refined here, 98%–99% of residues were in the core Ramachandran plot region as defined by Kleywegt and Jones [49]. Structures refined in this manner include RTRP(MYO2), RTHP(MYOCE), LTHP(MYO3), and LTHP(MYO4).

In order to assess the degree of modeling bias (discussed in Results and Discussion), structure factors for 1VXH were refined in-house using the protocol above. 1VXH had originally been refined using X-PLOR version 3.1 without crossvalidation. This rerefined structure is called RTRP(r1VXH).

Coordinates for 1A6K, 1VXH, 1VXE, and 1VXB were used without further refinement.

Acknowledgments

We thank Cayce Butler, Marcus Collins, Adam Finnefrock, Raphaël Kapfer, Emil Lobkovsky, Martin Novak, Matt Renzi, Mark Tate, Gil Toombes, and Weiru Wang for assistance in data collection; Richard Gillilan for help in data visualization; the MacCHESS staff, especially Bill Miller and Marian Szebenyi; Eric Brucker, Elaine Liong, and Wei Zhang for providing protein crystals; and Hans Frauenfelder and Robert H. Austin for useful discussions. We are grateful for the financial support of the Department of Energy (DE-FG02-97ER6244) and the NIH (NIH-AR-40252). CHESS is supported by an NSF National Facilities grant and the NIH Institute of General Medical Sciences via grant NSF-DMR97-13424. MacCHESS is supported by the NIH as a Research Resource (NIH-RR01646). Parts of this work are drawn from the PhD thesis of P.U., Princeton University, 2001.

Received: July 17, 2001
Revised: October 30, 2001
Accepted: November 13, 2001

References

1. Silva, J.L., and Weber, G. (1993). Pressure stability of proteins. Annu. Rev. Phys. Chem. *44*, 89–113.
2. Jonas, J., and Jonas, A. (1994). High-pressure NMR spectroscopy of proteins and membranes. Annu. Rev. Biophys. Biomol. Struct. *23*, 287–318.
3. Gross, M., and Jaenicke, R. (1994). Proteins under pressure: the influence of high hydrostatic pressure on structure, function, and assembly of proteins and protein complexes. Eur. J. Biochem. *221*, 617–630.
4. Bartlett, D.H., Kato, C., and Horikoshi, K. (1995). High pressure influences on gene and protein expression. Res. Microbiol. *146*, 697–706.
5. Mozhaev, V.V., Heremans, K., Frank, J., Masson, P., and Balny, C. (1996) High pressure effects on protein structure and function. Proteins *24*, 81–91.
6. Kundrot, C.E., and Richards, F.M. (1987). Crystal structure of hen egg-white lysozyme at a hydrostatic pressure of 1000 atmospheres. J. Mol. Biol. *193*, 157–170.

7. Kharakoz, D.P., and Sarvazyan, A.P. (1993). Hydrational and intrinsic compressibilities of globular proteins. Biopolymers *33*, 11–26.
8. Chalikian, T.V., Sarvazyan, A.P., and Breslauer, K.J. (1994). Hydration and partial compressibility of biological compounds. Biophys. Chem. *51*, 89–109.
9. Paci, E., and Velikson, B. (1997). On the volume of macromolecules. Biopolymers *41*, 785–797.
10. Richards, F.M. (1974). The interpretation of protein structures: total volume, group volume distributions, and packing density. J. Mol. Biol. *82*, 1–14.
11. Kundrot, C.E., and Richards, F.M. (1986). Collection and processing of X-ray diffraction data from protein crystals at high pressure. J. Appl. Crystallogr. *19*, 208–213.
12. Katrusiak, A., and Dauter, Z. (1996). Compressibility of lysozyme protein crystals by X-ray diffraction. Acta Crystallogr. *D52*, 607–608.
13. Fourme, R., Kahn, R., Mezouar, M., Girard, E., Hoerentrup, C., Prangé, T., and Ascone, I. (2001). High pressure protein crystallography (HPPX): instrumentation, methodology and results on lysozyme crystals. J. Synchrotron Radiat. *8*, 1149–1156.
14. Österberg, F. (1996) Induced Changes in the Diffuse X-Ray Scattering Background from Protein Crystals. PhD thesis, Princeton University, Princeton , New Jersey.
15. Thomanek, U.F., Parak, F., Mössbauer, R.L., Formanek, H., Schwager, P., and Hoppe, W. (1973). Freezing of myoglobin crystals at high pressure. Acta Crystallogr. *A29*, 263–265.
16. Tilton, R.F., Jr., and Petsko, G.A. (1988). A structure of sperm whale myoglobin at a nitrogen gas pressure of 145 atmospheres. Biochemistry *27*, 6574–6582.
17. Tilton, R.F., Jr. (1988). A fixture for X-ray crystallographic studies of biomolecules under high gas pressure. J. Appl. Crystallogr. *21*, 4–9.
18. Frauenfelder, H., Sligar, S.G., and Wolynes, P.G. (1991). The energy landscape and motions of proteins. Science *254*, 1598–1603.
19. Andrews, B.K., Romo, T., Clarage, J.B., Pettitt, B.M., and Phillips, G.N., Jr. (1998). Characterizing global substates of myoglobin. Structure *6*, 587–594.
20. Ansari, J., Berendzen, J., Braunstein, D., Cowen, B.R., Frauenfelder, H., Hong, M.K., Iben, I.E.T., Johnson, J.B., Ormos, P., Sauke, T.B., et al. (1987). Rebinding and relaxation in the myoglobin pocket. Biophys. Chem. *26*, 337–355.
21. Frauenfelder, H., McMahon, B.H., Austin, R.H., Chu, K., and Groves, J.T. (2001). The role of structure, energy landscape, dynamics, and allostery in the enzymatic function of myoglobin. Proc. Natl. Acad. Sci. USA *98*, 2370–2374.
22. Frauenfelder, H., Alberding, N.A., Ansari, A., Braunstein, D., Cowen, B.R., Hong, M.K., Iben, I.E.T., Johnson, J.B., Luck, S., Marden, M.C., et al. (1990). Proteins and pressure. J. Phys. Chem. *94*, 1024–1037.
23. Sage, J.T., Morikis, D., and Champion, P.M. (1991). Spectroscopic studies of myoglobin at low pH: heme structure and ligation. Biochemistry *30*, 1227–1237.
24. Yang, F., and Phillips, G.N., Jr. (1996). Crystal structure of CO-, deoxy-, and met-myoglobins at various pH values. J. Mol. Biol. *256*, 762–774.
25. Müller, J.D., McMahon, B.H., Chien, E.Y.T., Sligar, S.G., and Nienhaus, G.U. (1999). Connection between the taxonomic substates and protonation of histidines 64 and 97 in carbonmonoxy myoglobin. Biophys. J. *77*, 1036–1051.
26. Rabenstein, B., and Knapp, E.-W. (2001). Calculated pH-dependent population and protonation of carbon-monoxy-myglobin conformers. Biophys. J. *80*, 1141–1150.
27. Berman, H.M., Westbrook, J., Feng, Z., Gilliland, G., Bhat, T.N., Weissig, H., Shindyalov, I.N., and Bourne, P.E. (2000). The Protein Data Bank. Nucleic Acids Res. *28*, 235–242.
28. Vojtechovský, J., Chu, K., Berendzen, J., Sweet, R.M., and Schlichting, I. (1999) Crystal structures of myoglobin-ligand complexes at near-atomic resolution. Biophys. J. *77*, 2153–2174.
29. Kleywegt, G.J., and Jones, T. A. (2000) A super position. ESF/CCP4 Newsletter *31*, 9–14.
30. Teng, T.-Y., and Moffat, K. (1998). Cooling rates during flash cooling. J. Appl. Crystallogr. *31*, 252–257.
31. Kuriyan, J., Wilz, S., Karplus, M., and Petsko, G.A. (1986). X-ray structure and refinement of carbonmonoxy (Fe II)-myoglobin at 1.5 Å resolution. J. Mol. Biol. *192*, 133–154.
32. Oldfield, E., Guo, K., Augspurger, J.D., and Dykstra, C.E. (1991). A molecular model for the major conformational substates in heme proteins. J. Am. Chem. Soc. *113*, 7537–7541.
33. Austin, R.H., Beeson, K.W., Eisenstein, L., Frauenfelder, H., and Gunsalus, I.C. (1975). Dynamics of ligand binding in myoglobin. Biochemistry *14*, 5355–5373.
34. Jongeward, K.A., Magde, D., Taube, D.J., Marsters, J.C., Traylor, T.G., and Sharma, V.S. (1988). Picosecond and nanosecond geminate recombination of myoglobin with CO, O2, NO, and icocyanides. J. Am. Chem. Soc. *110*, 380–387.
35. Petrich, J.W., Lambry, J.-C., Kuczera, K., Karplus, M., Poyart, C., and Martin, J.-L. (1991). Ligand binding and protein relaxation in heme proteins: room temperature analysis of NO geminate recombination. Biochemistry *30*, 3975–3987.
36. Carver, T.E., Rohlfs, R.J., Olson, J.S., Gibson, Q.H., Blackmore, R.S., Springer, B.A., and Sligar, S.G. (1990) Analysis of the kinetic barriers for ligand binding to sperm whale myoglobin using site-directed mutagenesis and laser photolysis techniques. J. Biol. Chem. *265*, 20007–20020.
37. Gibson, Q.H., Olson, J.S., McKinnie, R.E., and Rohlfs, R.J. (1986). A kinetic description of ligand binding to sperm whale myoglobin. J. Biol. Chem. *261*, 10228–10239.
38. Olson, J.S., and Phillips, G.N., Jr. (1996). Kinetic pathways and barriers for ligand binding to myoglobin. J. Biol. Chem. *271*, 17593–17596.
39. Rejto, P.A., and Freer, S.T. (1996). Protein conformational substates from X-ray crystallography. Prog. Biophys. Mol. Biol. *66*, 167–196.
40. Kachalova, G.S., Popov, A.N., and Bartunik, H.D. (1999). A steric mechanism for inhibition of CO binding to heme proteins. Science *284*, 473–476.
41. Galkin, O., Buchter, S., Tabririan, A., and Schulte, A. (1997). Pressure effects on the proximal heme pocket in myoglobin probed by Raman and near-infrared absorption spectroscopy. Biophys. J. *73*, 2752–2763.
42. Garman, E.F., and Schneider, T.R. (1997). Macromolecular cryocrystallography. J. Appl. Crystallogr. *30*, 211–237.
43. Rossmann, M.G., and van Beek, C.G. (1999). Data processing. Acta Crystallogr. *D55*, 1631–1640.
44. CCP4 (Collaborative Computational Project 4) (1994). The CCP4 suite: programs for protein crystallography. Acta Crystallogr. *D50*, 760–763.
45. Brünger, A.T., Adams, P.D., Clore, G.M., DeLano, W.L., Gros, P., Grosse-Kunstleve, R.W., Jiang, J.-S., Kuszewski, J., Nilges, M., Pannu, N.S., et al. (1998). Crystallography & NMR system: a new software suite for macromolecular structure determination. Acta Crystallogr. *D54*, 905–921.
46. Brünger, A.T. (1992). Free R value: a novel statistical quantity for assessing the accuracy of crystal structures. Nature *355*, 472–475.
47. Jones, T.A., Zou, J.-Y., Cowan, S.W., and Kjeldgaard, M. (1991). Improved methods for building protein models in electron density maps and the location of errors in these models. Acta Crystallogr. *A47*, 110–119.
48. Laskowski, R.A., MacArthur, M.W., Moss, D.S., and Thornton, J.M. (1993). PROCHECK: a program to check the stereochemical quality of protein structures. J. Appl. Crystallogr. *26*, 283–291.
49. Kleywegt, G.J., and Jones, T.A. (1996). Phi/Psi-chology: Ramachandran revisited. Structure *4*, 1395–1400.

Accession Numbers

The coordinates and structure factors from this study have been deposited in the Protein Data Bank. These include 1JP6, 1JP8, 1JP9, and 1JPB for RTRP(MYO2), RTHP(MYOCE), LTHP(MYO3), and LTHP(MYO4), respectively.